Journal of Materials Chemistry A

PAPER

View Article Online
View Journal | View Issue

Cite this: J. Mater. Chem. A, 2015, 3, 7477

Control of micro/mesoporosity in non-hydrolytic hybrid silicophosphate xerogels†‡

Ales Styskalik,[ab] David Skoda,[ab] Zdenek Moravec,[a] Michal Babiak,[ab] Craig E. Barnes[c] and Jiri Pinkas*[ab]

Received 12th December 2014
Accepted 24th February 2015

DOI: 10.1039/c4ta06823h

www.rsc.org/MaterialsA

Non-hydrolytic sol–gel reactions of acetoxysilanes with trimethylsilyl esters of phosphoric and phosphonic acids produce cross-linked matrices containing homogeneous dispersions of silicon and phosphoryl groups connected together by networks of Si–O–P(=O) linkages. These polycondensation reactions proceed cleanly and under mild conditions for a wide variety of precursor silanes $R_nSi(OAc)_{4-n}$ (R = alkyl, aryl; n = 1, 2) and phosphoryl compounds $RP(O)(OSiMe_3)_2$ (R = alkyl, aryl) to provide hybrid xerogels, the final properties of which are a sensitive function of the organic substituents and the Si : P ratio of the precursors. The reactions of bridged acetoxysilanes $(AcO)_3Si–X–Si(OAc)_3$ and phosphoryl reagents $(Me_3SiO)_2P(O)–X–P(O)(OSiMe_3)_2$ have also been investigated and found to produce gels that exhibit large surface areas (up to 700 $m^2\ g^{-1}$). The presence of SiO_6 structural units in bridged-phosphoryl xerogels is related to their microporosity while the absence of such moieties in bridged-acetoxysilane networks is congruent with significant mesoporosity. Several important parameters are identified which can be used to tailor the properties of these hybrid matrices such that gels with specific polarity, porosity and surface area can be targeted at the time of synthesis.

1. Introduction

Sol–gel syntheses of organic–inorganic hybrid materials with covalently incorporated organic functionalities in silicate matrices have been studied with increasing interest for the application in and also in providing an extensive tool-box for the controlled fabrication of xerogels, nanoparticles, thin films and other advanced materials.[1–8] The refined procedures allow tailoring textural,[9,10] optical,[11] mechanical,[12,13] catalytic,[14,15] sensor,[16] and electrical properties.[17,18] Synthetic strategies rely, for example, on the copolymerization of metal alkoxide/oxide clusters functionalized with polymerizable groups with suitable co-monomers,[19–21] or on the controlled radical polymerization of polyhedral oligomeric silsesquioxanes (POSS).[22] Hybrid composites based on POSS precursors have reached the industrial scale of applications.[23–25] Furthermore, hydrolysis and condensation of alkyl- or aryltrialkoxysilanes provide single-phase organosilicagels composed of polysilsequioxane networks (so-called T-resins).[26] Despite the high number of reactive groups in these trifunctional organosilanes $RSiX_3$, their sol–gel polymerization products are incompletely condensed nonporous T-resins or the molecular polyhedral silsesquioxanes. However, network materials with high surface areas can be formed from $RSiX_3$ by co-condensation with monomers that contain a higher level of functionality, such as tetraethoxysilane (TEOS) or tetramethoxysilane (TMOS).

Two interconnected phenomena – surface area decrease and pore size increase – were observed in the hydrolytic sol–gel synthesis of silicagels from TEOS and trimethylethoxysilane, the latter of which was used as a condensation inhibitor.[27] Similar results were observed in the hydrolytic sol–gel co-polymerization of TEOS with alkyltrimethoxysilane $RSi(OMe)_3$.[28] In general, the bulkier the organic group R, the higher the decrease of surface area. Moreover, the different reactivities of $Si(OR)_4$ and $RSi(OR)_3$ in hydrolysis–condensation reactions at various pHs may preclude homogeneous incorporation and even lead to phase separation.[29]

Changing the precursor structure to bridged trialkoxysilanes $(RO)_3Si–X–Si(OR)_3$ gives rise to functional materials with controllable self-assembling properties[30–33] and mesoporous architectures.[34] By introducing hydrocarbon spacers X into the silicate network, properties such as hydrophobicity, porosity, UV-visible absorption and fluorescence, can be significantly modified. The morphology of a material can be controlled at the

[a]Masaryk University, Department of Chemistry, Kotlarska 2, CZ-61137 Brno, Czech Republic. E-mail: jpinkas@chemi.muni.cz; Fax: +420 549492443; Tel: +420 549496493

[b]Masaryk University, CEITEC MU, Kamenice 5, CZ-62500 Brno, Czech Republic

[c]University of Tennessee, Department of Chemistry, Knoxville, TN 37996-1600, USA

† Electronic supplementary information (ESI) available. CCDC 1038898. For ESI and crystallographic data in CIF or other electronic format see DOI: 10.1039/c4ta06823h

‡ Dedicated to Professor H. W. Roesky on the occasion of his 80th birthday.

molecular level by carefully designing suitable spacer groups that influence textural parameters. For example, an average pore diameter increases with longer alkylene spacers.[35]

Examples of non-hydrolytic preparations of hybrid xerogel materials in the present literature are much less common. Hay *et al.*[36] and Bourget *et al.*[37] used alkyhalogenide elimination from $RSiCl_3$ and $RSi(OEt)_3$ for the synthesis of organosilsesquioxane gels that were, however, nonporous. Non-hydrolytic condensations usually show better results in terms of homogeneity in mixed oxides, such as hybrid titania–silica xerogels also possessing high surface areas.[38–42] In general, it is not possible to predict how the precursor binding capacity and size of organic groups will influence the pore size and surface area in various final gel matrices and to discern some general trends. The preparation of homogeneous mixed oxides with controllable surface areas and pore size distribution through the introduction of organic groups still presents a challenge.

Hybrid silicophosphates are studied as promising materials for proton conducting membranes of fuel cells, gas sensors, and optical applications.[43–48] The synthesis of hybrid materials with an Si–O–P skeleton was accomplished by non-hydrolytic polycondensation induced by heating $RP(O)Cl_2$ (R = Me or Ph) with TEOS, or by their reaction with $SiCl_4$ in ^{t}BuOH.[49] Recently, preparation of low melting silicophosphate glasses has been described utilizing non-hydrolytic polycondensation with HCl elimination from anhydrous, solid H_3PO_4 or $RP(O)(OH)_2$ and alkyl-, aryl-, and vinylchlorosilanes, R_nSiCl_{4-n} ($n = 1, 2$), without employing any solvent.[50–53] However, the homocondensation and phase separation cannot be prevented in these systems. So far no porous hybrid organic–inorganic materials with an Si–O–P skeleton have been described.

We recently described a new non-hydrolytic ester elimination route to microporous silicophosphate xerogels with a purely inorganic framework by condensing silicon acetate, $Si(OAc)_4$, and tris(trimethylsilyl)phosphate, $OP(OSiMe_3)_3$ (TTP).[54] Optimization of reaction conditions leads to products with a high degree of condensation and large specific surface areas, while maintaining a homogeneous distribution of the components (eqn (1)).

$$3Si(OAc)_4 + 4OP(OSiMe_3)_3 \rightarrow Si_3P_4O_{16} + 12CH_3C(O)OSiMe_3 \quad (1)$$

Here we report on the application of this reaction principle to alkyl- and aryl-substituted silicon and phosphorus precursors to obtain hybrid materials with incorporated organic groups in the silicophosphate inorganic network with the aim to prepare mesoporous xerogels. In the first part, the reactions between TTP and acetoxysilanes $R_nSi(OAc)_{4-n}$ (R = alkyl, aryl; $n = 1, 2$) are investigated affording nonporous xerogels, oligomers, cyclic and cage molecules similar to silsesquioxanes. In the second part the changes of the surface area and pore size distribution are followed as a function of the molar ratios of reagents. Finally, completely new mesoporous silicophosphate xerogels are obtained by introducing bridging organic spacers into the network structure in the form of $(AcO)_3Si–X–Si(OAc)_3$ and $(Me_3SiO)_2P(O)–X–P(O)(OSiMe_3)_2$.

2. Experimental

2.1 General

All reactions and manipulations of the materials described here were performed in a dry N_2 atmosphere using Schlenk techniques or in dry nitrogen gloveboxes. Sources, procedures and characterization data for all solvents and reagents used in these investigations are summarized in the ESI† of this article.

2.2 General procedure for non-hydrolytic sol–gel reactions

The parent unmodified silicophosphate xerogel was prepared under conditions optimized to give the maximum surface area.[54] In a typical reaction, $OP(OSiMe_3)_3$ (TTP) was added dropwise to a stirred solution of $Si(OAc)_4$ (the molar ratio 4 : 3) in toluene to obtain a clear colorless gel (eqn (1)). The gel was aged at 80 °C for one week and then dried under vacuum for two days providing an opaque xerogel (**SiP**). Characterization and spectral analysis data of **SiP** were the same as reported previously.[54] Hybrid xerogels were synthesized in the same manner under the same conditions (toluene, concentration, and 80 °C) to estimate the influence of organic groups covalently bound to silicon and phosphorus (Sections 1, 2, and 3). Detailed experimental procedures for all the reactions of alkyl- and arylacetoxysilanes and alkylphosphonic acid esters can be found in the ESI† along with the characterization data for the obtained xerogels. Samples are denoted by abbreviations that point to the particular employed precursors as summarized in Table 1. For example, the abbreviation **SiP** denotes the reaction of $3Si(OAc)_4 + 4OP(OSiMe_3)_3$; **MeSiP**: $MeSi(OAc)_3 + OP(OSiMe_3)_3$; **SiP-MeSiX**: $Si(OAc)_4 + nMeSi(OAc)_3 + (1.33 + n)\ OP(OSiMe_3)_3$ ($n = 0–1$); **SiC1SiP**: $(AcO)_3Si–CH_2–Si(OAc)_3 + 2OP(OSiMe_3)_3$.

The organic byproduct of polycondensation was identified as trimethylsilylacetate by ^{1}H, ^{13}C NMR, and GC-MS.[54] NMR tube reactions between Si and P precursors were carried out to follow the reaction progress by ^{31}P NMR taken at 1, 24, and 168 h after the mixing of precursors in C_6D_6.

Tables 2–4 summarize the data for three different types of hybrid silicophosphate network solids prepared from (1) mono- and dialkyl/arylacetoxysilanes and alkyl/arylphosphonic acid esters, (2) co-condensation of $Si(OAc)_4$ and $OP(OSiMe_3)_3$ partially substituted with $R_nSi(OAc)_{4-n}$ ($n = 1, 2$; R = Me, Ph) and $PhP(O)(OSiMe_3)_2$, and (3) bridged acetoxysilanes and phosphonic acid esters. Detailed experimental procedures and characterization data (NMR, IR spectra) are provided in the ESI.†

3. Results and discussion

3.1 Mono- and dialkyl/arylacetoxysilanes and alkyl/arylphosphonic acid esters

A set of sol–gel reactions (80 °C, 168 h, and toluene or 100–130 °C, 2 h, and no solvent) and NMR tube reactions (r.t., C_6D_6) based on non-hydrolytic polycondensation of acetoxysilane and trimethylsilyl ester moieties was performed in order to evaluate the propensity of acetoxysilanes and phosphonic acid esters to condense and form gels as illustrated in Scheme 1. A 3-

Table 1 Abbreviations of precursors in non-hydrolytic sol–gel reactions

Abbreviation	Precursor	Abbreviation	Precursor
Si	$Si(OAc)_4$	**P**	$OP(OSiMe_3)_3$
MeSi	$MeSi(OAc)_3$	**SiCnSi**	$(AcO)_3Si–(CH_2)_n–Si(OAc)_3$
Me2Si	$Me_2Si(OAc)_2$	**HexP**	$C_6H_{11}P(O)(OSiMe_3)_2$
PhSi	$PhSi(OAc)_3$	**PhP**	$PhP(O)(OSiMe_3)_2$
Ph2Si	$Ph_2Si(OAc)_2$	**PC2P**	$(Me_3SiO)_2P(O)–(CH_2)_2–P(O)(OSiMe_3)_2$
BuSi	$^tBuSi(OAc)_3$	**PC6P**	$(Me_3SiO)_2P(O)–C_6H_4–P(O)(OSiMe_3)_2$
BuOSi	$^tBuOSi(OAc)_3$		

dimensionally cross-linked matrix of silicon centers and phosphoryl groups is formed. As the matrix grows and becomes more rigid, some acetate groups on silicon and trimethylsiloxy groups on phosphorus are presumed to become spatially isolated with one another within the matrix and are retained, thus reducing the average degree of condensation from 100%. The value of y then represents the number of uncondensed OAc and $SiMe_3$ groups.

The extent of condensation, followed by ^{31}P NMR (Fig. 1S†), allowed us to distinguish between the formation of molecular products, oligomers and polymers as summarized in Table 2S.† The condensation between Si and P precursors was confirmed by the formation of new NMR signals upfield from the starting esters. Signals of molecular and oligomeric condensation products then usually diminished and a broad signal of polymeric silicophosphates was observed (Fig. 1S†). No signals at a lower field from the starting phosphorus esters were observed attesting to the absence of ligand exchange and the consequent homocondensation.

In all reactions, the yield of the product as well as the mass of the starting precursors were precisely weighed to allow gravimetric estimation of the degree of condensation, DC, (Table 2, eqn (2)). Degree of condensation as defined by eqn (2) represents the relative difference between the maximum theoretical loss of Me_3SiOAc in comparison to what is experimentally observed. This difference also defines the number of acetoxy groups on silicon and trimethylsilyl ester groups on phosphorus that are left in the matrix. n_{total} is the number of moles of organic groups in the starting materials and $n_{residual}$ is the molar amount of residual organic groups in the xerogel computed from the difference of the theoretical and the experimental yield. The condensation reactions were never quantitative, therefore DC was used for calculating the theoretical mass loss for thermogravimetric experiments (ML_{calc})

Table 2 Mono- and dialkyl/arylacetoxysilanes and alkyl/arylphosphonic acid esters: reagent molar ratios, degrees of condensation (DC) and comparison of experimental (ML) and calculated mass losses (ML_{calc}) during thermogravimetric analysis of hybrid silicophosphates

Sample	n_{Si} [mmol]	n_P [mmol]	DC [%]	ML [%]	ML_{calc} [%]
SiP	1.0	1.33	85.7	29.4	32.8
MeSiP	1.0	1.0	87.1	32.1	35.3
Me2SiP	1.0	0.67	89.4	—	—
PhSiP	1.0	1.0	63.6	—	—
Ph2SiP	1.0	0.7	61.9	—	—
BuSiP	1.0	1.1	69.3	—	—
SiHexP	1.0	2.0	100	65.0	42.8
SiPhP	1.0	2.0	58.1	63.5	64.1

Table 3 Co-condensation of $Si(OAc)_4$ and $OP(OSiMe_3)_3$ partially substituted with $R_nSi(OAc)_{4-n}$ (n = 1, 2; R = Me, Ph) and $PhP(O)(OSiMe_3)_2$: reagent stoichiometry, degrees of condensation (DC) and comparison of experimental (ML) and calculated mass losses (ML_{calc}) during thermogravimetric analysis of xerogels with partially substituted $Si(OAc)_4$ or $OP(OSiMe_3)_3$

Sample	x^a	DC [%]	ML [%]	ML_{calc} [%]
SiP	—	85.7	29.4	32.8
SiP-MeSi1	0.19	79.2	35.3	41.4
SiP-MeSi2	0.29	80.7	31.6	39.7
SiP-MeSi3	0.37	82.0	30.6	38.0
SiP-MeSi4	0.51	83.8	29.1	35.6
SiP-MeSi5	1.24	91.0	31.5	24.1
SiP-Me2Si1	0.08	74.8	26.6	46.0
SiP-Me2Si2	0.17	85.3	29.9	33.5
SiP-Me2Si3	0.21	88.2	36.5	27.1
SiP-Me2Si4	0.28	84.9	29.1	34.0
SiP-Me2Si5	0.37	87.5	28.6	—
SiP-Me2Si6	0.44	83.1	30.2	36.4
SiP-PhSi1	0.53	83.7	34.6	39.2
SiP-PhSi2	0.97	81.0	34.9	44.7
SiP-Ph2Si1	0.11	81.0	33.6	41.5
SiP-Ph2Si2	0.32	80.3	38.0	45.3
SiP-PhP1	0.35	83.0	28.2	39.6
SiP-PhP2	1.49	87.3	47.3	41.2

[a] Amount of added organosilane/phosphonate components according to eqn (4)–(6).

Table 4 Bridged acetoxysilanes and phosphonic acid esters: degrees of condensation (DC) and comparison of experimental (ML) and calculated mass losses (ML_{calc}) during thermogravimetric analysis of xerogels with bridging organic groups

Sample	DC [%]	ML [%]	ML_{calc} [%]
SiC1SiP	85.6	27.2	29.3
SiC2SiP	78.1	35.3	27.4
SiC3SiP	88.5	36.8	31.3
SiC6SiP	—	45.9	—
SiPC2P	83.6	31.9	32.9
SiPC6P	77.0	33.9	47.7

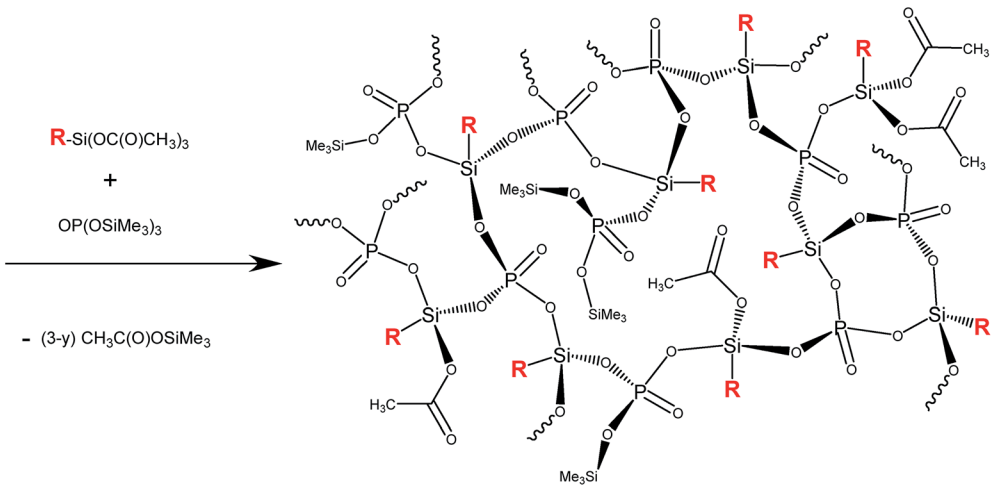

Scheme 1 Polycondensation of alkyl/arylacetoxysilanes and $OP(OSiMe_3)_3$, R = methyl, phenyl, or ^{t}butyl.

assuming the removal of residual OAc and $SiMe_3$ groups upon heating.

$$DC = 100(n_{total} - n_{residual})/n_{total} \quad (2)$$

While the degree of condensation results for silicophosphate samples containing methyl groups from $MeSi(OAc)_3$ were similar to that of the parent **SiP** xerogel (85–89%), the introduction of large organic groups (phenyl or ^{t}butyl) significantly lowered the DC to 58–69%. This was also reflected in the physical appearance of the products – while the **MeSiP** sample formed a hard glass, **PhSiP**, **Ph2SiP** and **BuSiP** samples were isolated as viscous oils after drying. As a result of incomplete condensation, residual Me_3SiOP and CH_3COOSi groups were present in the products as deduced from the IR and NMR spectra of xerogels (Scheme 1).

The stability of Si–C and P–C bonds in these reactions was confirmed by the IR and solid-state NMR studies of the products (see below) as there is no evidence of Si–C or P–C bond rupture. One can expect that the ability of these precursors to form porous xerogels would be lower in comparison with the parent reaction of $Si(OAc)_4$ and TTP in analogy to trifunctional aryltrialkoxysilanes (*e.g.* $PhSi(OEt)_3$) that in classical hydrolytic sol–gel reactions preferentially form oligosilsesquioxanes rather than gels. At high monomer concentrations, however, gels with low specific surface areas can be prepared by heating or with the addition of a strong base.[55]

Covalently bound organic groups caused significant changes in the morphological properties of products in comparison with the parent **SiP** xerogel (Table 2S†). Only systems with $MeSi(OAc)_3$, $C_6H_{11}P(O)(OSiMe_3)_2$ and $PhP(O)(OSiMe_3)_2$ formed gels, which were nonporous. Once the organic group attached to Si is too bulky (phenyl or ^{t}butyl) or the number of alkyl/aryl substituents is increased (dimethyldiacetoxysilane instead of methyltriacetoxysilane), the ability to form gels is completely lost and the reactions yield oligomeric mixtures. The glue-like products were heated at 250 °C in an oven under nitrogen to promote further condensation of the acetoxy- and trimethylsiloxy-groups. This resulted in the formation of insoluble, polymeric and hard non-porous (BET) glasses similar to low-melting glasses obtained by solventless condensation between alkyl/arylchlorosilanes and H_3PO_4 (100%).[50–53]

The reaction of TTP and diphenyldiacetoxysilane (Table 2S,† eqn (3)) produced a mixture of molecular products. One of them crystallized out of the reaction mixture and was isolated. This compound has been spectroscopically characterized and the molecular structure was determined by the single crystal X-ray diffraction analysis (Fig. 1). In this molecular product, condensation stops when a $Si_2P_2O_4$ ring is formed according to eqn (3). Relevant metric data are gathered in Tables 3S and 4S in the ESI.† The core of the structure is a centrosymmetric $Si_2P_2O_4$ ring in a chair conformation similar to what is observed in $[\{^tBu_2Si\{O_2P(O)Ph\}\}_2]$.[56]

$$2Ph_2Si(OAc)_2 + 2OP(OSiMe_3)_3 \rightarrow [(Ph_2Si\{O_2P(O)OSiMe_3\})_2] + 4Me_3SiOAc \quad (3)$$

From the presented results, it can be concluded that the organic groups attached to Si have a stronger effect on the polycondensation reaction than the ones bound to the P center, *e.g.* the condensation reaction between phenyltriacetoxysilane and TTP stopped at the stage of oligomers, while replacing one reactive Me_3SiO-group on P in TTP with a phenyl group resulted in the formation of a polymer (Table 2S†). Understanding the reason for this different behavior would potentially allow one to design gels with specific properties. This hypothesis was investigated with the help of IR and solid-state NMR spectroscopic studies of the prepared xerogels.

The IR spectra of **SiP** xerogel[54] display important vibration bands at 1771, 1721, and 1541 cm^{-1} which are assigned to the $\nu_{as}(COO)$ stretches of acetates; the band at 1541 cm^{-1} arises from the bidentate bridging form (Fig. 2).[57,58] Strong CH_3 symmetric bending and rocking vibrations at 1259 and 854/764 cm^{-1} are characteristic of the $SiMe_3$ groups.[59] A medium intensity shoulder at 1300 cm^{-1} represents the P=O terminal

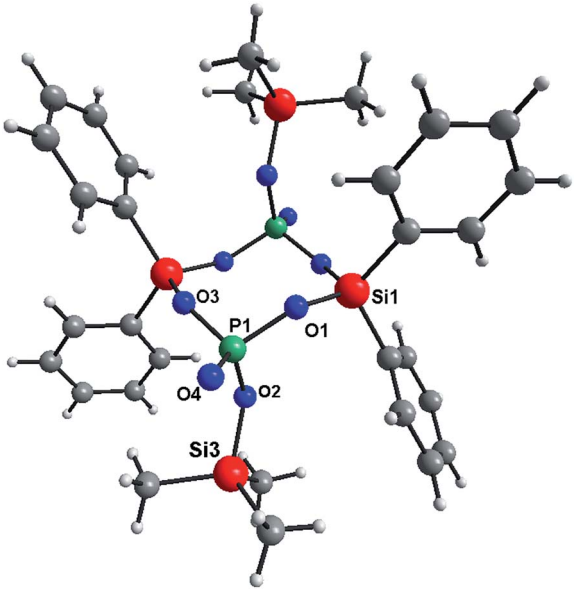

Fig. 1 Molecular structure of $[(Ph_2Si\{O_2P(O)OSiMe_3\})_2]$.

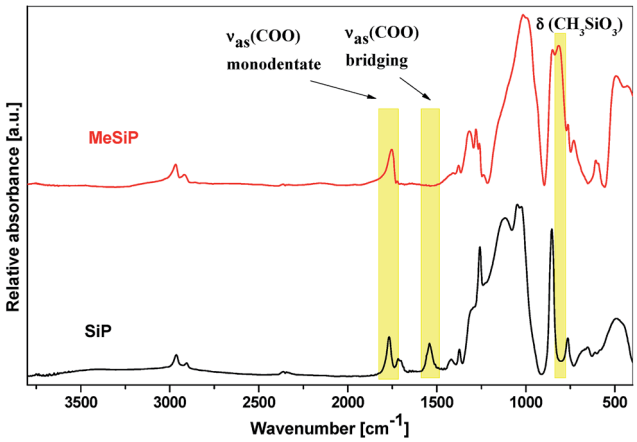

Fig. 2 IR spectra of a hybrid silicophosphate xerogels with CH_3–SiO_3 groups (**MeSiP**, the top) and the parent silicophosphate (**SiP**, the bottom).

bonds[60,61] and finally a strong composite band at 1129 cm^{-1} serves as a benchmark for the predominant formation of Si–O–P bonds.[62,63] The IR spectra of hybrid xerogels with organic groups bound to silicon (**MeSiP** to **BuSiP**, Table 2) feature characteristic bands for residual organic groups (1771 and 1721 cm^{-1} for acetates; 1259 and 854/764 cm^{-1} for Me_3Si groups), but they differ in certain features (Fig. 2): (i) the characteristic vibrations of CH_3–SiO_3 groups (ρCH_3Si 815 and 732 cm^{-1}) are present in **MeSiP** (that are separate from the absorption bands of the residual Me_3SiOP groups), (ii) vibrations of aromatic ν $C_{ar}H$ at 3052 cm^{-1} feature in the **PhSiP** and **Ph2SiP** spectra (Fig. 2S†), (iii) the vibration band of bidentate acetate at 1540 cm^{-1} is missing in all xerogels containing Si–C bonds, and (iv) the strong composite band, which appears in the **SiP** sample between 900 and 1350 cm^{-1}, is now significantly sharper and is located from 900 to 1200 cm^{-1}. These observations indicate that acetate and the P=O groups do not coordinate with silicon and do not form bridges in the hybrid gels (Scheme 1). The absence of these binding modes was additionally corroborated by solid-state NMR (see below). Finally, the changes in the internal structure of these gels correlate with important structural and morphological properties of the hybrid gels.

Further evidence for the structural changes deduced from IR data was found in the solid-state NMR spectra of the hybrid silicophosphate xerogels. First, the broad ^{31}P signal of $P(OSi)_4$ moieties observed in the parent **SiP** xerogels shifted downfield by 10 ppm to −37 ppm indicating the loss of the coordinative P=O→Si bonds (Chart 1B). Therefore the signal was assigned to the $O{=}P(OSi)_3$ groups (Chart 1A). No other signal was observed in the ^{31}P MAS NMR spectra (Fig. 3S†). The ^{13}C signals of the bridging acetates (in **SiP** at 16.3 and 190.6 ppm)[54] disappeared and only resonances belonging to unidentate acetates (at 22.7 and 169.7 ppm), CH_3–SiO_3 groups (1.1 ppm) and residual Me_3SiOP (−4.1 ppm) groups were present (Fig. 4S†). As a consequence of the missing P=O→Si and C=O→Si bridges, signals for six-coordinate silicon species were absent in the ^{29}Si CPMAS NMR spectra which now featured only signals of CH_3–SiO_3 groups (−61 ppm, T^3) and residual Me_3SiOP (26 ppm, M) (Fig. 3). All the above described phenomena were also observed in solution NMR spectra of oligomeric samples **Me2SiP**, **PhSiP** and **BuSiP**. In other words, the number of the maximum possible Si–O–P connections available to form a network decreased from 6 (Chart 1B) to 3 (Chart 1A) in the case of silicon and from 4 (Chart 1B) to 3 (Chart 1A) for phosphorus, significantly influencing the structure (oligomers *vs.* xerogels, low cross-linking) and specific surface area of xerogels (Table 2S†).

On the other hand, the structures of xerogels synthesized from $RP(O)(OSiMe_3)_2$, R = Ph (**SiPhP**) or C_6H_{11} (**SiHexP**), and $Si(OAc)_4$ are similar to the parent **SiP** material. According to ^{31}P MAS NMR, terminal P=O bonds are converted to the P=O→Si moieties (Chart 1C and D, Fig. 3S†).

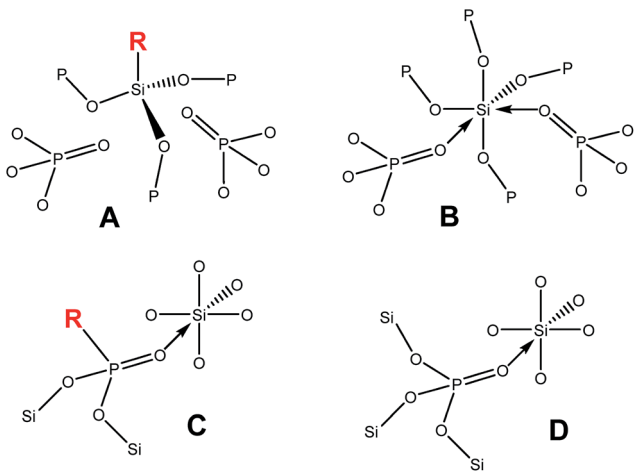

Chart 1 Coordination environments of Si atoms in silicophosphate xerogels.

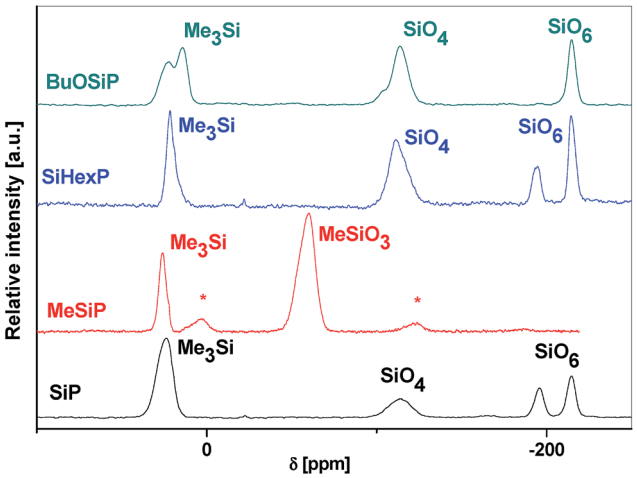

Fig. 3 ^{29}Si CPMAS NMR spectra of hybrid xerogels with $(CH_3)_3C–O–SiO_3$ groups (**BuOSiP**), $C_6H_{11}–P(O)O_2$ groups (**SiHexP**), $CH_3–SiO_3$ groups (**MeSiP**) and the parent silicophosphate sample (SiP). Asterisks denote spinning side bands.

Moreover, some CH_3COO groups become bidentate (as confirmed by IR and ^{13}C MAS NMR spectra, Fig. 4S†) by coordinating to Si, and thus there are two types of six-coordinate silicon atoms as confirmed by the ^{29}Si MAS NMR spectra of **SiPhP** and **SiHexP** xerogels (Fig. 3). No evidence of a P–C bond rupture was observed. However, the resulting xerogels were non-porous.

The question why $R_nSi(OAc)_{4-n}$ precursors do not achieve hexacoordination around silicon was puzzling. It can be seen from Table 2S,† that steric effects play a significant role during condensation reactions. While $MeSi(OAc)_3$ yields a gel, $PhSi(OAc)_3$ produces a mixture of oligomers. Similarly $Me_2Si(OAc)_2$ with $OP(OSiMe_3)_3$ afforded oligomeric species, while $Ph_2Si(OAc)_2$ under the same conditions yielded a mixture of molecular products. Considering these facts, there is a question, if the methyl group in $MeSi(OAc)_3$ causes such a steric hindrance at silicon that the hexacoordination is not possible, or if there are any other effects, which prevent silicon from becoming hypercoordinated. Furthermore the electron donor properties of methyl groups must be considered. Electron rich methyl groups could reduce the positive charge on silicon and lower its Lewis acidity.

In order to distinguish electronic *versus* steric effects, the condensation employing ^{t}BuOSi(OAc)$_3$ and $OP(OSiMe_3)_3$ was investigated (**BuOSiP**). In ^{t}butoxytriacetoxysilane, only OAc groups undergo condensation, the electronic environment of Si closely resembles that in silicon tetraacetate (*i.e.* SiO_4), and the bulky ^{t}BuO-groups will cause a strong steric hindrance of the silicon center and possibly suppress hexacoordination. Under standard reaction conditions, polycondensation was rather slow in comparison with $Si(OAc)_4$ and did not afford any gel. While unreacted starting TTP was observed together with trimethylsilylacetate among volatile byproducts, neither ^{t}butylacetate nor ^{t}butoxytrimethylsilane were identified by GC-MS which excluded any elimination of ^{t}BuO-groups. Six-coordinate $Si(OP)_6$ was, however, clearly evidenced by a resonance at −215 ppm in the ^{29}Si CPMAS NMR spectrum (Fig. 3) of the isolated solid product. Interestingly, the acetates maintained their unidentate nature since no other signal, such as that of the $Si(OP)_4(O{=}C)_2$ species at −195 ppm,[54] appeared in the spectrum. These results were supported by ^{13}C CPMAS NMR and IR spectroscopy showing the absence of bridging acetates (ESI†). To conclude, the bulky ^{t}BuO-groups slowed condensation reactions but did not affect the ability of silicon atoms to acquire hexacoordination. This property of silicon is therefore controlled by its Lewis acidity.

3.2 Co-condensation of $Si(OAc)_4$ and $OP(OSiMe_3)_3$ partially substituted with $R_nSi(OAc)_{4-n}$ (n = 1, 2; R = Me, Ph) and $PhP(O)(OSiMe_3)_2$

We subsequently turned our attention to systems in which substituents were added to both silicon ($R_nSi(OAc)_{4-n}$ ($n = 1, 2$)) and phosphorus ($PhP(O)(OSiMe_3)_2$), which were expected to yield products with high surface areas.[1,55,64,65] It is well known that in hydrolytic sol–gel reactions the differences in reactivity at various pHs for $Si(OR)_4$ and $RSi(OR)_3$ may preclude homogeneous incorporation and frequently lead to a precipitous loss of surface areas in the resulting products.[29] We have also investigated the effect of partially substituting $Si(OAc)_4$ with alkyl- and arylacetoxysilanes (Tables 3 and 6S†) according to eqn (4) and (5) and also $OP(OSiMe_3)_3$ with $PhP(O)(OSiMe_3)_2$ (eqn (6)). Hybrid networks containing a homogeneous dispersion of organic groups within the xerogel were expected as observed in Section 1.

$$(3 - x)Si(OAc)_4 + 4/3xRSi(OAc)_3 + 4OP(OSiMe_3)_3 \rightarrow (1 - x/3)Si_3P_4O_{16}\cdot(4/3x)RSiPO_4 + 12AcOSiMe_3 \quad (4)$$

$$(3 - x)Si(OAc)_4 + 2xR_2Si(OAc)_2 + 4OP(OSiMe_3)_3 \rightarrow (1 - x/3)Si_3P_4O_{16}\cdot(2x/3)R_6Si_3P_2O_8 + 12AcOSiMe_3 \quad (5)$$

$$3Si(OAc)_4 + (4 - x)OP(OSiMe_3)_3 + 3/2xPhP(O)(OSiMe_3)_2 \rightarrow (1 - x/4)Si_3P_4O_{16}\cdot(3/4x)SiPh_2P_2O_6 + 12AcOSiMe_3 \quad (6)$$

The structure of the resulting xerogels was strongly related to the parent **SiP** samples. The IR spectra of hybrid xerogels showed almost no changes with respect to the parent **SiP** gel and featured all characteristic vibrations described earlier. The ^{13}C CPMAS NMR spectra displayed the presence of organic groups covalently bound to silicon (methyl or phenyl) consistent with the incorporation of the alkyl- or arylsilane components into the gel products. Finally, the ^{29}Si CPMAS NMR spectra showed one additional resonance representing the particular $MeSiO_3/Me_2SiO_2/PhSiO_3/Ph_2SiO_2$ groups in addition to the signals of the residual Me_3SiOP and SiO_4 and two types of SiO_6 moieties for each product (Fig. 5S–7S†).

All of the gel products listed in Table 6S† exhibited significant surface areas (isotherms shown in the ESI, Fig. 8S–14S†). The surface area decreased substantially with the increasing amount of organic groups (Table 6S,† Fig. 4) in agreement with the similar reports on the hydrolytic sol–gel reactions.[28] Two effects can be discerned: (i) the bulkier the organic group, the steeper the decrease of the surface area (*e.g.*

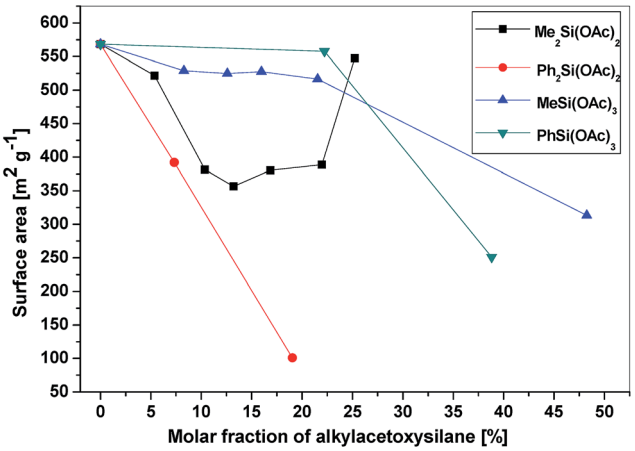

Fig. 4 Dependence of the surface area of the hybrid xerogels on the molar fraction of alkyl/arylacetoxysilanes.

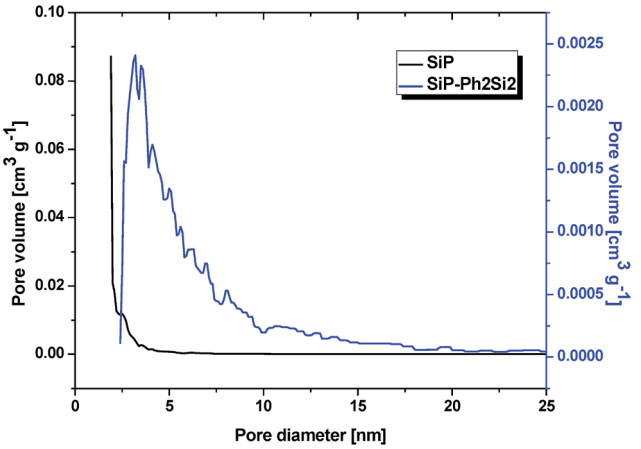

Fig. 6 Pore size distributions of **SiP** and **SiP-Ph2Si2** xerogels (DFT Kernel used: N_2 at 77 K on silica, a cylindrical pore, and NSDFT equilibrium model).

dimethyldiacetoxysilane *vs.* diphenyldiacetoxysilane); (ii) the lower the number of potential cross-link bonds, the steeper the decrease of surface areas in xerogels with low contents of the alkyl/arylacetoxysilane additive (*e.g.* phenyltriacetoxysilane *vs.* diphenyldiacetoxysilane). In the xerogels with high contents of dimethyldiacetoxysilane, there is a significant increase of the surface area (from 356 $m^2\ g^{-1}$ at 13 mol% of $Me_2Si(OAc)_2$ to 547 $m^2\ g^{-1}$ at 25 mol%). However, the volatile organic byproducts contained unreacted dimethyldiacetoxysilane which apparently does not enter the network structure of the gel but acts only as a template. It is eliminated from the pores after the reaction during drying *in vacuo*, leading to progressively higher surface areas. A similar phenomenon was observed in the case of nonvolatile diphenyldiacetoxysilane, where the surface area of products with a high molar ratio of phenyl groups increased significantly, but only after washing the xerogel with toluene. The washings contained diphenyldiacetoxysilane, $[(Ph_2Si\{O_2P(O)OSiMe_3\})_2]$, and other molecular condensation products with TTP. In contrast, hybrid silicophosphates synthesized from methyltriacetoxysilane and phenyltriacetoxysilane contained no unreacted alkyl/arylacetoxysilanes or some molecular condensation products occluded in the xerogels. Fig. 5 illustrates the dependence of the average pore size on the content of alkyl/arylacetoxysilanes. Interestingly, the average pore size increases as a function of the size of organic groups and the number of bonds silicon can form with phosphorus in these gels. This observation is important, because the **SiP** xerogel has an average pore size just on the boundary between micropores and mesopores (2.0 nm) and is mostly microporous (*ca.* 70%), while the hybrid organic–inorganic materials with 20% of $R_nSi(OAc)_{4-n}$ are mostly mesoporous (0% microporosity for **SiP-MeSi4**, **SiP-PhSi1** and **SiP-Ph2Si2**). This phenomenon is clearly seen in Fig. 6, where a comparison of DFT pore size distributions of **SiP** and **SiP-Ph2Si2** samples is shown. The general trends allow us to control the surface area and pore sizes in these hybrid xerogels.

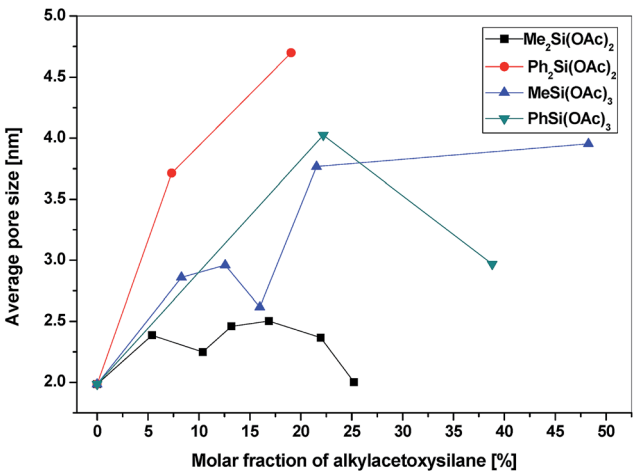

Fig. 5 Dependence of the average pore size of the hybrid xerogels on the molar fraction of alkyl/arylacetoxysilanes.

To compare the effects of organic groups bound to Si and P, the bis(trimethylsilyl)phenyl phosphonate was introduced into the xerogel in amounts of 13 and 47 mol% replacing TTP (Table 6S:† **SiP-PhP1** and **SiP-PhP2**). As in the case of $PhSi(OAc)_3$ and other $R_nSi(OAc)_{4-n}$ ($n = 1, 2$) precursors, the specific surface area decreased in a similar manner, but the mean pore size stayed small around 2.0 nm and the sample displayed 70% microporosity similar to the unsubstituted **SiP** sample (Table 6S†). Thus, in contrast to alkyl/arylacetoxysilanes, the phosphonate influenced only the surface area, but did not play a significant role in influencing the mean pore size and micro/mesoporosity of the xerogels. These observations indicate that the mesoporosity was introduced by adding $RSiO_3$ and R_2SiO_2 units of alkyl/arylacetoxysilanes, while the microporosity is strongly related to the presence of SiO_6 groups, which are formed from TTP as well as from phosphonates (Chart 1B and C).

3.3 Bridged acetoxysilanes and phosphonic acid esters

Bis(trialkoxysilyl)alkanes with flexible alkylene spacers are prone to intra- or intermolecular cyclization which hinders the network formation and increases gelation time.[66] While rigid

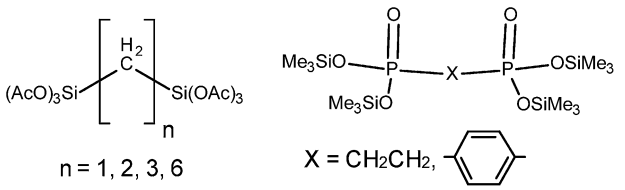

Chart 2 Precursors for hybrid silicophosphate xerogels with bridging organic groups.

spacer groups produce porous xerogels, flexible ones with a hydrocarbon chain longer than six carbons generally cause pore collapse. Also higher DC produces a less compliant network which is in turn more porous.

To increase the surface area of xerogels we tested, as the sources of silicon and phosphorus, various bridged bifunctional molecules (Chart 2). An advantage of these bridged precursors is that they are not able to self-condense and form cyclic molecules[66] that would impede the gelation process. Homocondensations resulting in acetic acid anhydride or hexamethyldisiloxane elimination are not feasible under reaction conditions used here. All these precursors afforded rigid, colorless (milky) and transparent gels within a short reaction period. They formed two completely different classes of xerogels: (i) hybrid silicophosphates with bridging groups between Si atoms and (ii) hybrid silicophosphates with bridging groups between P atoms. These two classes of xerogels differ in structural and textural properties as will be shown below.

From the results presented above, one can expect that the network of xerogels based on $(AcO)_3Si(CH_2)_nSi(OAc)_3$, $n = 1$–3, 6, will be built from tetrahedral $(CH_2)_nSiO_3$ and $O{=}PO_3$ units as in the **MeSiP** and **PhSiP** samples (Scheme 1 and Chart 1A). The ^{29}Si CPMAS NMR spectra, in fact, displayed only two resonances at −64.5 ppm ($(CH_2)_nSiO_3$) and 25.6 ppm (residual Me_3SiOP) with no evidence for the SiO_6 centers and no evidence of Si–C bond cleavage. Also the ^{31}P and ^{13}C MAS NMR and IR spectra were similar to **MeSiP** supporting their structural similarity (Fig. 15S–17S†). However, the introduction of the bridging molecules with six acetate groups provided an abundant cross-linking, so that the surface area increased significantly in comparison with the **MeSiP** sample (Table 5).

The surface area of the xerogels ranges from 369 to 703 m^2 g^{-1} and reaches its maximum for the 1,2-ethanediyl bridging unit. Longer spacers exhibit lower surface areas (Table 5). All the samples with bridging units between Si atoms are mesoporous, in contrast to the **SiP** sample, with the mean pore sizes ranging from 3.7 to 11.9 nm (Fig. 21S†). These observations support our suggestion that the microporosity in silicophosphate xerogels is dependent on the presence of the SiO_6 units while mesoporous materials can be obtained by restricting the Si coordination to 4. The average pore size increases with the increasing length of the aliphatic chain for $n = 1$–3 and then drops down for $n = 6$ probably because of the non-rigidity of the bridging unit (Table 5). These results are similar to those observed by Oviatt *et al.*,[35] where average pore sizes increased from 4.09 nm to 19.7 nm and the surface area simultaneously decreased from 684 to 88 m^2 g^{-1} on going from bis(triethoxysilyl)butane to bis(triethoxysilyl)decane in the case of base-catalyzed hydrolytic sol–gel condensations.

Completely different structural and textural properties were displayed by the hybrid silicophosphates with the bridging group between P atoms. These materials were strongly related to **SiP**, **SiP-PhP1**, and **SiP-PhP2** samples. The bridging organic groups bound to phosphorus did not hinder the formation of hexacoordinated silicon (Chart 1C) and both MAS NMR and IR spectra closely resembled the **SiP** samples including the evidence for SiO_6 groups, while no P–C bond rupture was observed (Fig. 15S–17S†). These xerogels reached the maximum surface area of 617 m^2 g^{-1} and their average pore sizes were on the boundary between micro- and mesoporosity (2.2 and 2.1 nm), similar to the **SiP** samples. The content of the micropore surface area was around 50% (Table 5). The textural diversity caused by the location of the organic spacer (between the Si *vs.* P atoms) is clearly seen in the comparison of adsorption–desorption isotherms of the corresponding xerogels (Fig. 7, Fig. 18S–20S†). The **SiPC6P** sample did not show any hysteresis and the main gas adsorption proceeded at low relative pressures similarly as in the **SiP** sample.[54] In contrast, the isotherm of the **SiC2SiP** sample was of the type IV and displayed hysteresis H3 in medium relative pressures corroborating the mesoporosity of these xerogels.

3.4 Thermal properties of the hybrid silicophosphate xerogels

The elimination and oxidation of organic groups and crystallization of silicon phosphates from the **SiP** sample upon heating in air were described previously.[54] The experimental mass losses (ML) for most of the hybrid silicophosphates are in reasonable agreement with the calculated ones (ML_{calc})

Table 5 Textural properties of xerogels with bridging organic groups

Sample	Si source	P source	SA [m^2 g^{-1}]	V_{total} [cm^3 g^{-1}]	D^a [nm]	MP^b [%]
SiCSiP	$(AcO)_3SiCH_2Si(OAc)_3$	$OP(OSiMe_3)_3$	505	0.462	3.7	0
SiC2SiP	$(AcO)_3Si(CH_2)_2Si(OAc)_3$	$OP(OSiMe_3)_3$	703	1.559	9.0	0
SiC3SiP	$(AcO)_3Si(CH_2)_3Si(OAc)_3$	$OP(OSiMe_3)_3$	369	1.091	11.9	0
SiC6SiP	$(AcO)_3Si(CH_2)_6Si(OAc)_3$	$OP(OSiMe_3)_3$	385	0.753	7.5	0
SiPC2P	$Si(OAc)_4$	$(Me_3SiO)_2P(O)CH_2CH_2P(O)(OSiMe_3)_2$	553	0.296	2.2	51
SiPC6P	$Si(OAc)_4$	$(Me_3SiO)_2P(O)C_6H_4P(O)(OSiMe_3)_2$	617	0.328	2.1	52

[a] Average pore diameters ($4V_{total}$/SA). [b] Determined by the *t*-plot.

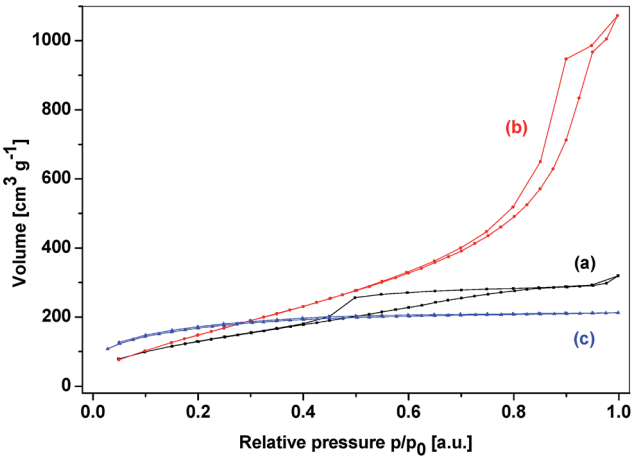

Fig. 7 Adsorption–desorption isotherms of xerogels (a) SiC1SiP, (b) SiC2SiP and (c) SiPC6P.

from DC (Tables 2–4). Three exothermic weight loss steps were observed, identically as in the **SiP** xerogel. They appeared for all the samples in these ranges: from 50 to 250 °C, from 500 to 600 °C and between 900 and 990 °C. Samples with covalently bound phenyl groups showed one more mass loss between 300 and 500 °C apparently caused by the degradation of aromatic rings.

The crystallization of $Si_5P_6O_{25}$ from the **SiP** xerogel was observed as early as at 150 °C and was accompanied by a decrease in the surface area. Also the hybrid samples were heated in air in order to describe the textural properties of heated xerogels. All the samples displayed the breakdown of the porous structure and rapid decrease of the surface area upon heating to 200 °C for 4 h. The highest surface area after calcination was only 20 $m^2\ g^{-1}$ for the sample **SiP-MeSi3** (the parent xerogel 528 $m^2\ g^{-1}$). The hybrid samples after TG analysis were amorphous, only some of them contained small amounts of crystalline silicon orthophosphate (PDF 40-457) or cubic silicon diphosphate (PDF 12-1321).

4. Conclusions

This work extends our previous efforts to synthesize homogenous silicophosphates which were prepared by a non-hydrolytic sol–gel polycondensation reaction based on acetic acid ester elimination.[54] While the reactions of silicon tetraacetate and tris(trimethylsilyl)phosphate provided microporous gels with SiO_6 structural units, the introduction of organic groups in the form of different alkyl/arylacetoxysilanes induced structural and textural changes leading to nonporous hybrid silicophosphate glasses. Such a drastic change of properties was ascribed to the lowering of the cross-linking capacity of silicon. Moreover, the organo-substituted silicon centers were shown not to be sufficiently Lewis acidic to acquire hexacoordination while steric hindrance did not play a major role in preventing the formation of SiO_6 moieties. The reaction of $OP(OSiMe_3)_3$ with $Ph_2Si(OAc)_2$ afforded only molecular products of condensation in contrast to other alkyl/arylacetoxysilanes. One of them, $[(Ph_2Si\{O_2P(O)OSiMe_3\})_2]$, was isolated and its structure was determined by single crystal X-ray diffraction analysis.

Partially substituting $Si(OAc)_4$ with $R_nSi(OAc)_{4-n}$ (n = 1, 2; R = Me, Ph) and varying the nature of the organic group R allowed us to tune the surface area in the range from 101 to 568 $m^2\ g^{-1}$ and average pore sizes from 2.0 to 4.7 nm in resulting xerogels. $R_2Si(OAc)_2$ and acetoxysilanes with bulky organic groups caused a bigger decrease of the surface area and average pore size increase in comparison to $RSi(OAc)_3$ and acetoxysilanes with small substituents. However the products were still significantly microporous.

Finally, the introduction of bridging organic groups provided an additional number of cross-linking possibilities which was reflected in the increase of the surface area of the xerogels. The organic spacer between silicon atoms caused the disappearance of the SiO_6 units similar to alkyl/arylacetoxysilanes. This structural change was accompanied by a change in textural properties – these samples were completely mesoporous with a highest surface area of 703 $m^2\ g^{-1}$ and an average pore size of 9.0 nm for the C_2H_4 bridge. The length of the bridging unit of $(AcO)_3Si(CH_2)_nSi(OAc)_3$ significantly influenced the pore size distribution – the average pore size increased with the increasing number of carbon atoms in the organic spacer for n = 1 to 3. In the case of the substitution of TTP by $(Me_3SiO)_2P(O)CH_2CH_2P(O)(OSiMe_3)_2$ and $(Me_3SiO)_2P(O)C_6H_4$-$P(O)(OSiMe_3)_2$, the structures of the xerogels were still predominantly built up of the SiO_6 units and displayed a significant microporosity reaching the highest surface area at 617 $m^2\ g^{-1}$ with an average pore size of 2.1 nm in the case of the phenylene bridge. These results point to a significant difference in the properties of xerogels built from units with spacer groups between silicon atoms in contrast to the spacers between phosphorus atoms.

Acknowledgements

The authors thank the project CEITEC – Central European Institute of Technology CZ.1.05/1.1.00/02.0068, KONTAKT II LH11028, GACR GAP207/11/0555 and Single Crystal X-Ray Diffraction Core Facility for financial assistance. J.P. thanks the Fulbright Foundation for a scholarship. A.S. thanks the Brno City Municipality for Brno a Ph.D. Talent Scholarship.

References

1 D. A. Loy and K. J. Shea, *Chem. Rev.*, 1995, **95**, 1431–1442.
2 G. Cerveau and R. J. P. Corriu, *Coord. Chem. Rev.*, 1998, **178–180**(2), 1051–1071.
3 C. Sanchez, F. Ribot and B. Lebeau, *J. Mater. Chem.*, 1999, **9**, 35–44.
4 R. J. P. Corriu, *Angew. Chem., Int. Ed.*, 2000, **39**, 1376–1398.
5 G. Kickelbick, *Hybrid Materials: Synthesis, Characterization, and Applications*, John Wiley & Sons, 2007.
6 C. Sanchez, L. Rozes, F. Ribot, C. Laberty-Robert, D. Grosso, C. Sassoye, C. Boissiere and L. Nicole, *C. R. Chim.*, 2010, **13**, 3–39.

7 C. Sanchez, K. J. Shea and S. Kitagawa, *Chem. Soc. Rev.*, 2011, **40**, 471–472.
8 D. A. Loy, K. A. Obrey-DeFriend, K. V. Wilson Jr, M. Minke, B. M. Baugher, C. R. Baugher, D. A. Schneider, G. M. Jamison and K. J. Shea, *J. Non-Cryst. Solids*, 2013, **362**, 82–94.
9 G. Cerveau, R. J. P. Corriu and E. Framery, *Polyhedron*, 2000, **19**, 307–313.
10 W. Chaikittisilp, M. Kubo, T. Moteki, A. Sugawara-Narutaki, A. Shimojima and T. Okubo, *J. Am. Chem. Soc.*, 2011, **133**, 13832–13835.
11 C. Sanchez, B. Lebeau, F. Chaput and J.-P. Boilot, *Adv. Mater.*, 2003, **15**, 1969–1994.
12 Y. Tokudome, T. Sato, M. Hidaka and M. Takahashi, *J. Sol-Gel Sci. Technol.*, 2013, **65**, 318–323.
13 H. Dong, R. F. Reidy and J. D. Brennan, *Chem. Mater.*, 2005, **17**, 6012–6017.
14 A. P. Wight and M. E. Davis, *Chem. Rev.*, 2002, **102**, 3589–3614.
15 M. Sebah, S. P. Maddala, P. Haycock, A. Sullivan, H. Toms and J. Wilson, *J. Mol. Catal. A: Chem.*, 2013, **374–375**, 59–65.
16 N. A. Carrington and Z.-L. Xue, *Acc. Chem. Res.*, 2007, **40**, 343–350.
17 L. Brigo, V. Auzelyte, K. A. Lister, J. Brugger and G. Brusatin, *Nanotechnology*, 2012, **23**, 325302.
18 F. Eckstorff, Y. Zhu, R. Maurer, T. E. Müller, S. Scholz and J. A. Lercher, *Polymer*, 2011, **52**, 2492–2498.
19 U. Schubert, N. Huesing and A. Lorenz, *Chem. Mater.*, 1995, **7**, 2010–2027.
20 C. Sanchez, C. Boissiere, S. Cassaignon, C. Chaneac, O. Durupthy, M. Faustini, D. Grosso, C. Laberty-Robert, L. Nicole, D. Portehault, F. Ribot, L. Rozes and C. Sassoye, *Chem. Mater.*, 2014, **26**, 221–238.
21 G. Fornasieri, L. Rozes, S. Le Calvé, B. Alonso, D. Massiot, M. N. Rager, M. Evain, K. Boubekeur and C. Sanchez, *J. Am. Chem. Soc.*, 2005, **127**, 4869–4878.
22 J. Pyun and K. Matyjaszewski, *Chem. Mater.*, 2001, **13**, 3436–3448.
23 G. Li, L. Wang, H. Ni and C. U. Pittman, *J. Inorg. Organomet. Polym.*, 2001, **11**, 123–154.
24 J. D. Lichtenhan, *Comments Inorg. Chem.*, 1995, **17**, 115–130.
25 D. B. Cordes, P. D. Lickiss and F. Rataboul, *Chem. Rev.*, 2010, **110**, 2081–2173.
26 R. Corriu, *Polyhedron*, 1998, **17**, 925–934.
27 S. Lin, C. Ionescu, E. M. Valliant, J. V. Hanna, M. E. Smith and J. R. Jones, *J. Mater. Chem.*, 2010, **20**, 1489.
28 R. Al-Oweini, *Appl. Surf. Sci.*, 2010, **257**, 276.
29 K. Nakanishi and K. Kanamori, *J. Mater. Chem.*, 2005, **15**, 3776–3786.
30 B. Boury, R. J. P. Corriu, V. Le Strat, P. Delord and M. Nobili, *Angew. Chem., Int. Ed.*, 1999, **38**, 3172–3175.
31 G. Creff, G. Arrachart, P. Hermet, H. Wadepohl, R. Almairac, D. Maurin, J.-L. Sauvajol, C. Carcel, J. J. E. Moreau, P. Dieudonné, M. W. C. Man and J.-L. Bantignies, *Phys. Chem. Chem. Phys.*, 2012, **14**, 5672–5679.
32 G. Creff, B. P. Pichon, C. Blanc, D. Maurin, J.-L. Sauvajol, C. Carcel, J. J. E. Moreau, P. Roy, J. R. Bartlett, M. Wong Chi Man and J.-L. Bantignies, *Langmuir*, 2013, **29**, 5581–5588.
33 B. Boury and R. J. P. Corriu, *Chem. Commun.*, 2002, 795–802.
34 F. Hoffmann, M. Cornelius, J. Morell and M. Fröba, *Angew. Chem., Int. Ed.*, 2006, **45**, 3216–3251.
35 H. W. Oviatt, K. J. Shea and J. H. Small, *Chem. Mater.*, 1993, **5**, 943–950.
36 J. N. Hay, D. Porter and H. M. Raval, *J. Mater. Chem.*, 2000, **10**, 1811–1818.
37 L. Bourget, D. Leclercq and A. Vioux, *J. Sol-Gel Sci. Technol.*, 1999, **14**, 137–147.
38 A. Styskalik, D. Skoda, J. Pinkas and S. Mathur, *J. Sol-Gel Sci. Technol.*, 2012, **63**, 463–472.
39 O. Lorret, V. Lafond, P. H. Mutin and A. Vioux, *Chem. Mater.*, 2006, **18**, 4707–4709.
40 D. P. Debecker and P. H. Mutin, *Chem. Soc. Rev.*, 2012, **41**, 3624–3650.
41 L. Crouzet, D. Leclercq, P. Mutin and A. Vioux, *J. Sol-Gel Sci. Technol.*, 2003, **26**, 335–338.
42 P. H. Mutin and A. Vioux, *J. Mater. Chem. A*, 2013, **1**, 11504–11512.
43 M. Nogami, H. Matsushita, Y. Goto and T. Kasuga, *Adv. Mater.*, 2000, **12**, 1370–1372.
44 A. Matsuda, T. Kanzaki, K. Tadanaga, M. Tatsumisago and T. Minami, *Solid State Ionics*, 2002, **154&155**, 687–692.
45 M. Mika, M. Paidar, B. Klapste, M. Masinova, K. Bouzek and J. Vondrak, *J. Phys. Chem. Solids*, 2007, **68**, 775–779.
46 J.-M. Lim, J.-H. Won, H.-J. Lee, Y. T. Hong, M.-S. Lee, C. H. Kod and S.-Y. Lee, *J. Mater. Chem.*, 2012, **22**, 18550–18557.
47 M. Takahashi, M. Suzuki, Y. Miyagawa, R. Ihara, Y. Tokuda, T. Yoko, T. Nemoto and S. Isoda, *J. Sol-Gel Sci. Technol.*, 2010, **54**, 319–324.
48 I. N. Tsvetkova, O. A. Shilova, M. G. Voronkov, Y. P. Gomza and K. M. Sukhoy, *Glass Phys. Chem.*, 2011, **34**, 68–76.
49 R. J. P. Corriu, D. Leclercq, P. H. Mutin, L. Sarlin and A. Vioux, *J. Mater. Chem.*, 1998, **8**, 1827–1833.
50 M. Mizuno, M. Takahashi, Y. Tokuda and T. Yoko, *Chem. Mater.*, 2006, **18**, 2075–2080.
51 Y. Tokuda, Y. Tanaka, M. Takahashi, R. Ihara and T. Yoko, *J. Ceram. Soc. Jpn.*, 2009, **117**, 842–846.
52 H. Niida, Y. Tokuda, M. Takahashi, T. Uchino and T. Yoko, *J. Non-Cryst. Solids*, 2002, **311**, 145–153.
53 M. Mizuno, M. Takahashi, Y. Tokuda and T. Yoko, *J. Sol-Gel Sci. Technol.*, 2007, **44**, 47–52.
54 A. Styskalik, D. Skoda, Z. Moravec, J. G. Abbott, C. E. Barnes and J. Pinkas, *Microporous Mesoporous Mater.*, 2014, **197**, 204–212.
55 D. W. Schaefer, G. Beaucage, D. A. Loy, K. J. Shea and J. S. Lin, *Chem. Mater.*, 2004, **16**, 1402–1410.
56 Y. Vaugeois, R. D. Jaeger, J. Levalois-Mitjaville, A. Mazzah, M. Wörle and H. Grützmacher, *New J. Chem.*, 1998, **22**, 783–785.
57 N. W. Alcock, V. M. Tracy and T. C. Waddington, *J. Chem. Soc., Dalton Trans.*, 1976, 2243.
58 B. P. Straughan, W. Moore and R. McLaughlin, *Spectrochim. Acta, Part A*, 1986, **42**, 451–456.

59 Y. Song, Y. Huang, E. A. Havenga and I. S. Butler, *Vib. Spectrosc.*, 2001, **27**, 127–134.
60 V. G. Plotnichenko, V. O. Sokolov, V. V. Koltashev and E. M. Dianov, *J. Non-Cryst. Solids*, 2002, **306**, 209–226.
61 E. M. Dianov, V. V. Koltashev, V. G. Plotnichenko, V. O. Sokolov and V. B. Sulimov, *J. Non-Cryst. Solids*, 1999, **249**, 29–40.
62 N. Shibata, M. Horigudhi and T. Edahiro, *J. Non-Cryst. Solids*, 1981, **45**, 115–126.
63 J. Wong, *J. Non-Cryst. Solids*, 1976, **20**, 83–100.
64 K. J. Shea, D. A. Loy and O. Webster, *J. Am. Chem. Soc.*, 1992, **114**, 6700–6710.
65 R. J. P. Corriu, J. J. E. Moreau, P. Thepot and M. W. C. Man, *Chem. Mater.*, 1992, **4**, 1217–1224.
66 K. J. Shea and D. A. Loy, *Acc. Chem. Res.*, 2001, **34**, 707–716.